Electronic Supplementary Information (ESI) for

What impact does ammonia have on the microstructure of the precursor and the electrochemical performance of Ni-rich layered oxides?

Jilu Zhang[1,2,†], Xinyue Zhai[1,3,†], Tian Zhao[1], Xiaoxia Yang[1], Qin Wang[1,4], Zhongjun Chen[5], Meng-Cheng Chen[6], Jian-Jie Ma[6], Ying-Rui Lu[7], Sung-Fu Hung[6], Weibo Hua[1,2,4,*]

[1] School of Chemical Engineering and Technology, Xi'an Jiaotong University, No.28, West Xianning Road, Xi'an, Shaanxi 710049, China. Email: weibo.hua@xjtu.edu.cn.

[2] Institute for Applied Materials (IAM), Karlsruhe Institute of Technology (KIT), Hermann-von-Helmholtz-Platz 1, D-76344 Eggenstein-Leopoldshafen, Germany.

[3] National innovation platform (Centre) for Industry-Education Integration of Energy Storage Technology, Xi'an Jiaotong University, No.28, West Xianning Road, Xi'an, Shaanxi 710049, China.

[4] School of Chemical Engineering, Sichuan University, No. 24 South Section 1, Yihuan Road, 610065, Chengdu, China.

[5] Beijing Synchrotron Radiation Facility, Institute of High Energy Physics, Chinese Academy of Sciences, Beijing, China.

[6] Department of Applied Chemistry and Center for Emergent Functional Matter Science, National Yang Ming Chiao Tung University, Hsinchu 300, Taiwan.

[7] National Synchrotron Radiation Research Center, Hsinchu 300, Taiwan.

† These authors contributed equally to this work.

S1 Calculations

Crystallization kinetic

Steady state crystallization kinetics were calculated using a continuously operated Mixed-Suspension Mixed-Product Removal (MSMPR) crystallizer which is very similar to the CSTR. As this method allows for the simultaneous determination of both the growth rate and the nucleation rate. With negligible crystal breakage and agglomeration effects, the equilibrium equations for the population of a continuous MSMPR crystallizer during the stabilization phase can be described as follows:

$$\frac{d(Gn)}{dL} + \frac{n}{\tau} = 0 \tag{1}$$

where G is the overall crystal growth rate, n is the population density, L is the crystal size, and τ is the mean residence time. The size distribution and shape of all crystals are the same in steady-state operation of the MSMPR crystalliser. The size of all crystal nuclei is zero.

Since the co-precipitated particles exhibited "size-dependent" growth, the crystal growth kinetics were analyzed on the basis of the Abegg, Stevens and Larson (ASL) growth rate equation:

$$G(L) = G^0(1 + \gamma L)^b \tag{2}$$

where G^0 is the nucleus growth rate, γ is determined by $\gamma = 1/G^0\tau$ and b is an empirical parameter. Thus, the size-dependent liner growth rate $(L) = dL/d\tau$ can be simplified to the following equation:

$$\frac{d(nG(L))}{dL} = -\frac{n}{\tau} \tag{3}$$

In combination with these equations, the population balance can be integrated as follows:

$$n = n^0(1+\gamma L)^{-b} exp\left[\frac{1-(1+\gamma L)^{1-b}}{1-b}\right] \quad (4)$$

The population density of particles in the crystalline steady state is calculated by the following equation:

$$n_i = \frac{M_T \Delta V_i}{k_v \rho_c \Delta L_i \bar{L}_i^3} \quad (5)$$

where is M_T the suspension density, ΔV_i is the volume fraction of solids, k_v is the volume shape factor, ρ_c is the solid density, ΔL_i is length of i channel, $\bar{L}_i^3$ is the average particle size of the i channel.

Finally, the G^0 values in both crystallisers can be calculated from the population density map of the precursors. Therefore, the nucleation rate (B^0) can also be derived from the following equation:

$$B^0 = n^0 G^0 \quad (6)$$

Li-ion diffusion coefficient

The Li-ion diffusion coefficient (D_{Li+}) of the electrodes during the first cycle was measured using the Galvanostatic intermittent titration technique (GITT) method. The current was interrupted after a duration of 20 min (τ) and relaxed for 3 h to reach a new steady state potential E_s, from which the change in the steady state voltage ΔE_s (=E_s − E_0) over the galvanostatic titration can be determined. This process was repeated over a voltage interval of 2.7-4.3 V. Based on the GITT measurements, D_{Li+} can be calculated from the following equation

$$D_{Li^+} = \frac{4}{\pi t}\left(\frac{m_B V_M}{M_B S}\right)^2 \left(\frac{\Delta E_s}{\Delta E_\tau}\right)^2 \quad (7)$$

where m_B is the mass of the active material, V_m is the molar volume of the electrode material, M_B is the relative Molecular mass, S is the effective surface area of the electrode in contact with the electrolyte, t is the time, ΔE_τ is derived from the total change in cell voltage to eliminate iR drop during the constant current pulse τ of the one-step GITT experiment.

Apparent activation energy

Nyquist plots of the pristine samples were collected at 298.15, 308.15, 318.15 and 328.145 K (**Figure S12**) to calculate the activation energy (E_a) by the following Arrhenius equation:

$$i_0 = RT/nFR_{ct} \quad (8)$$

$$i_0 = Aexp(-E_a/RT) \quad (9)$$

Here i_0 is the exchange current, R_{ct} is charge transfer impedance, R is the gas constant, T (K) is the absolute temperature, A is a temperature-independent coefficient, n is the number of transferred electrons, and F is the Faraday constant. The linear plot of $\ln(i_0/A)$ versus 1/T is derived and then the activation energy was calculated ($E_a = -Rk$, where k is the slope of the fitting line).

S2 Additional results and discussion

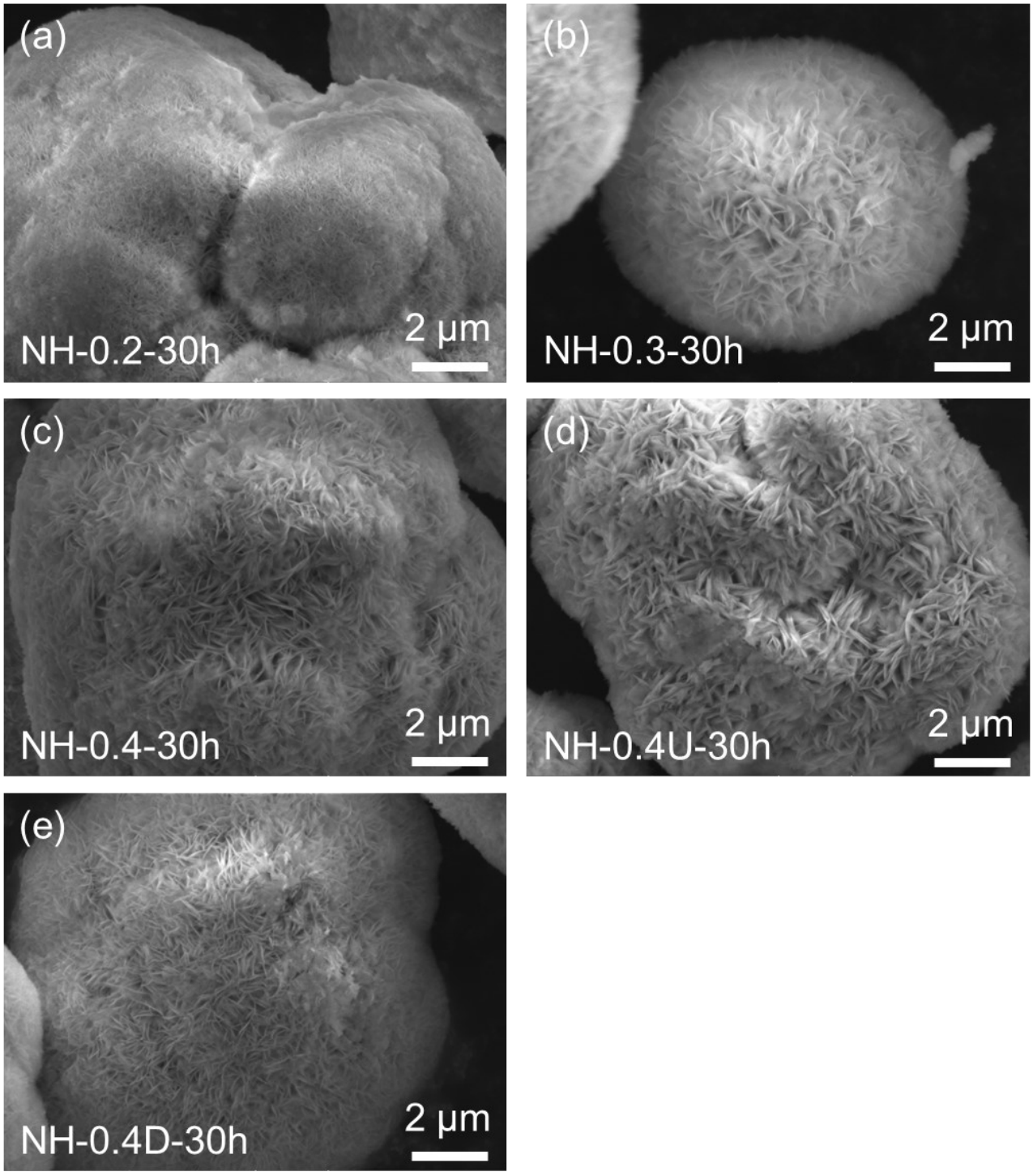

Figure S1. SEM images of (a) NH-0.2, (b) NH-0.3, (c) NH-0.4, (d) NH-0.4U and (e) NH-0.4D after 30 hours of reaction.

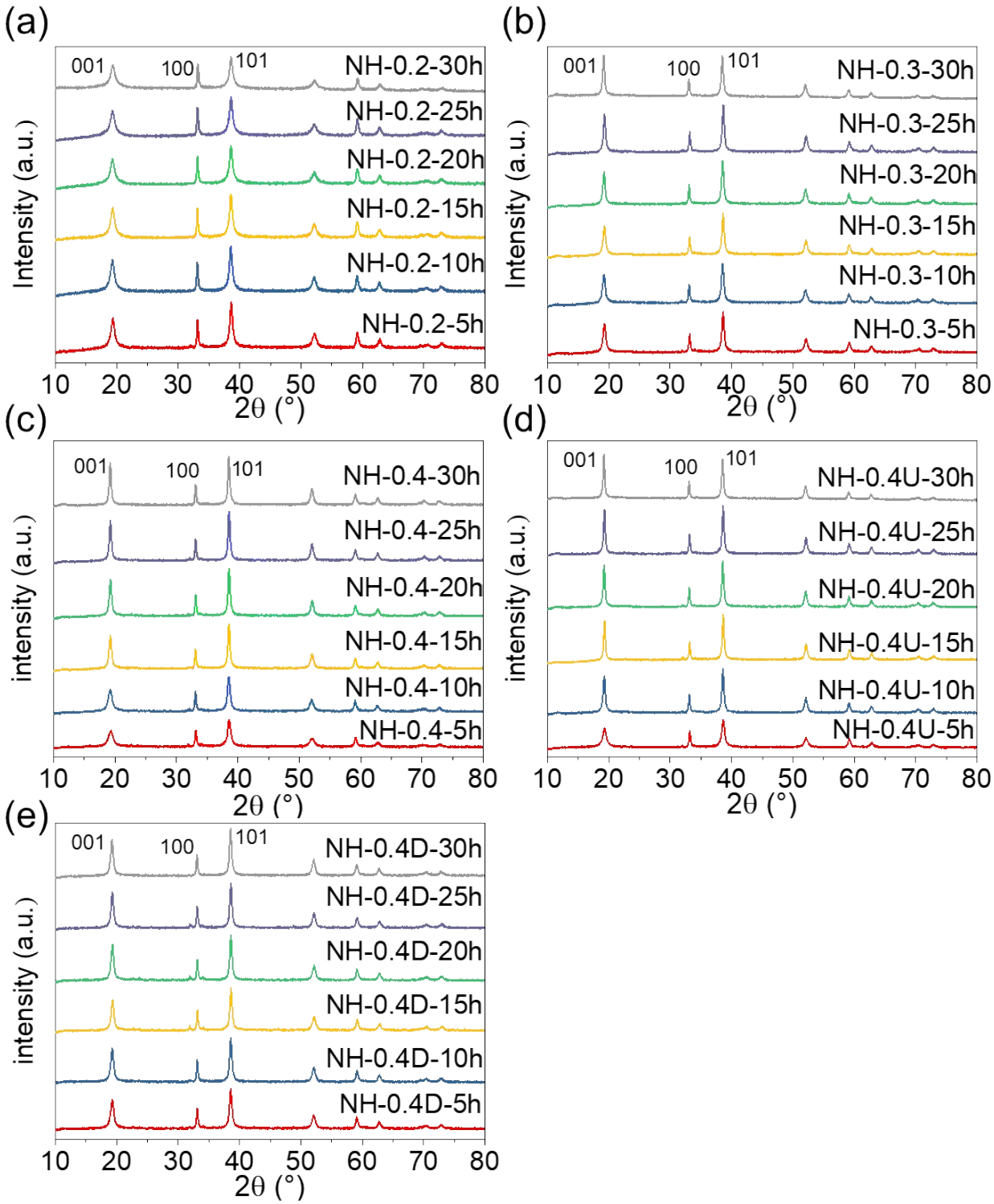

Figure S2. XRD pattern images of (a) NH-0.2, (b) NH-0.3, (c) NH-0.4, (d) NH-0.4U and (e) NH-0.4D at different co-precipitation reaction time (5 – 30 h).

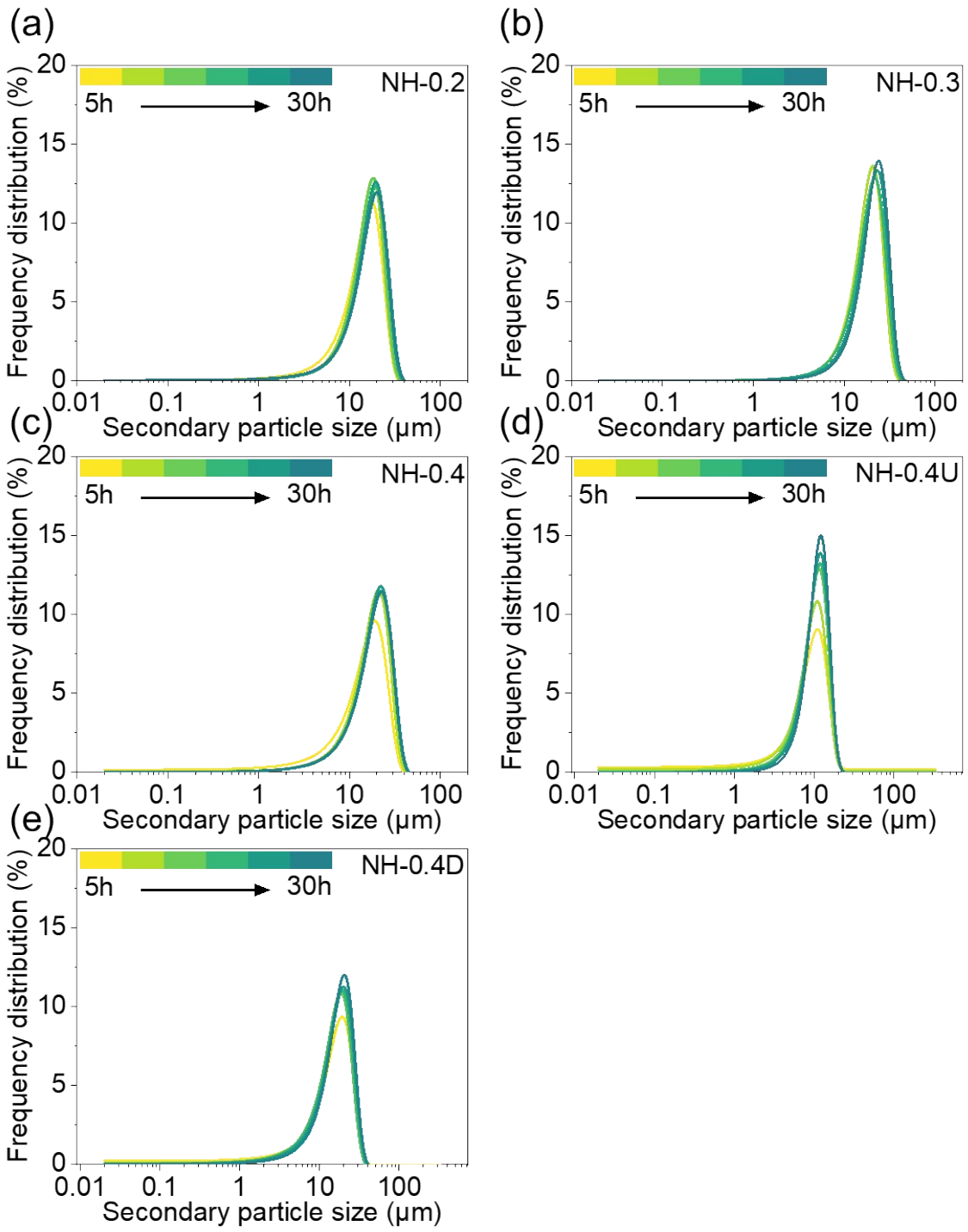

Figure S3. Secondary particles size distribution of (a) NH-0.2, (b) NH-0.3, (c) NH-0.4, (d) NH-0.4U and (e) NH-0.4D at different co-precipitation reaction time (5 – 30 h).

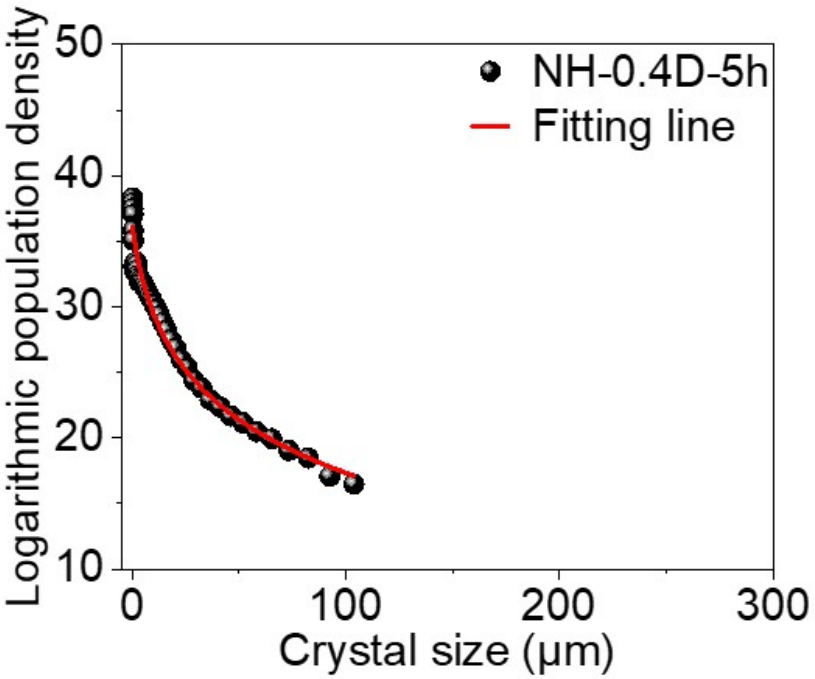

Figure S4. The population density distribution plots and ASL fitting results.

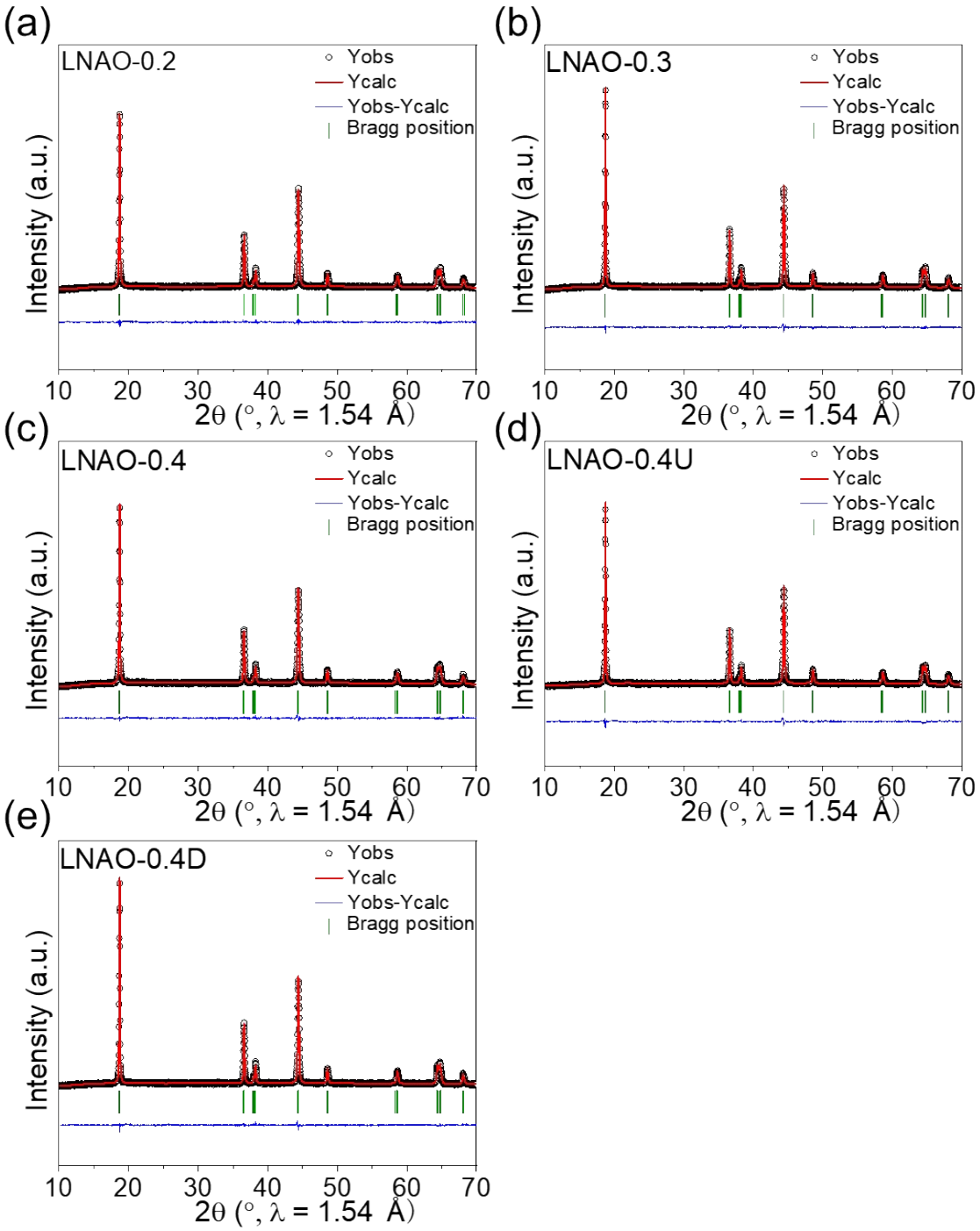

Figure S5. Rietveld refinement XRD patterns of (a) LNAO-0.2, (b) LNAO-0.3, (c) LNAO-0.4, (d) LNAO-0.4U and (e) LNAO-0.4D.

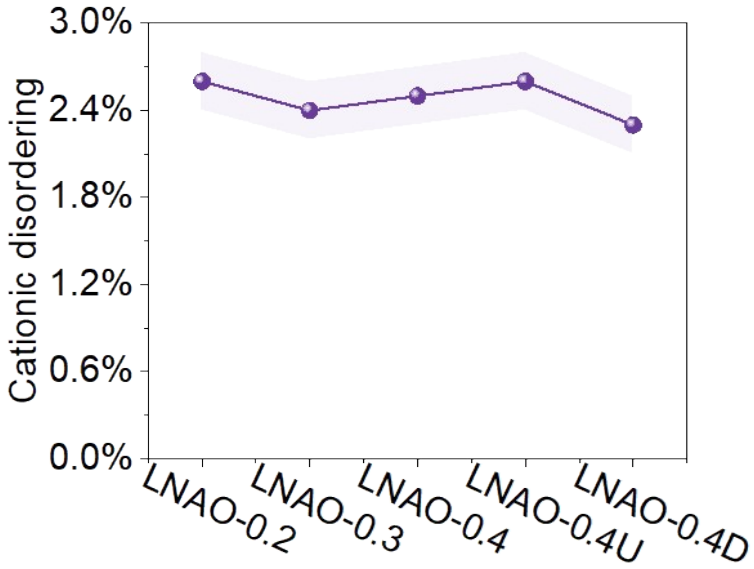

Figure S6. Changes in the degree of cation disorder in layered structures.

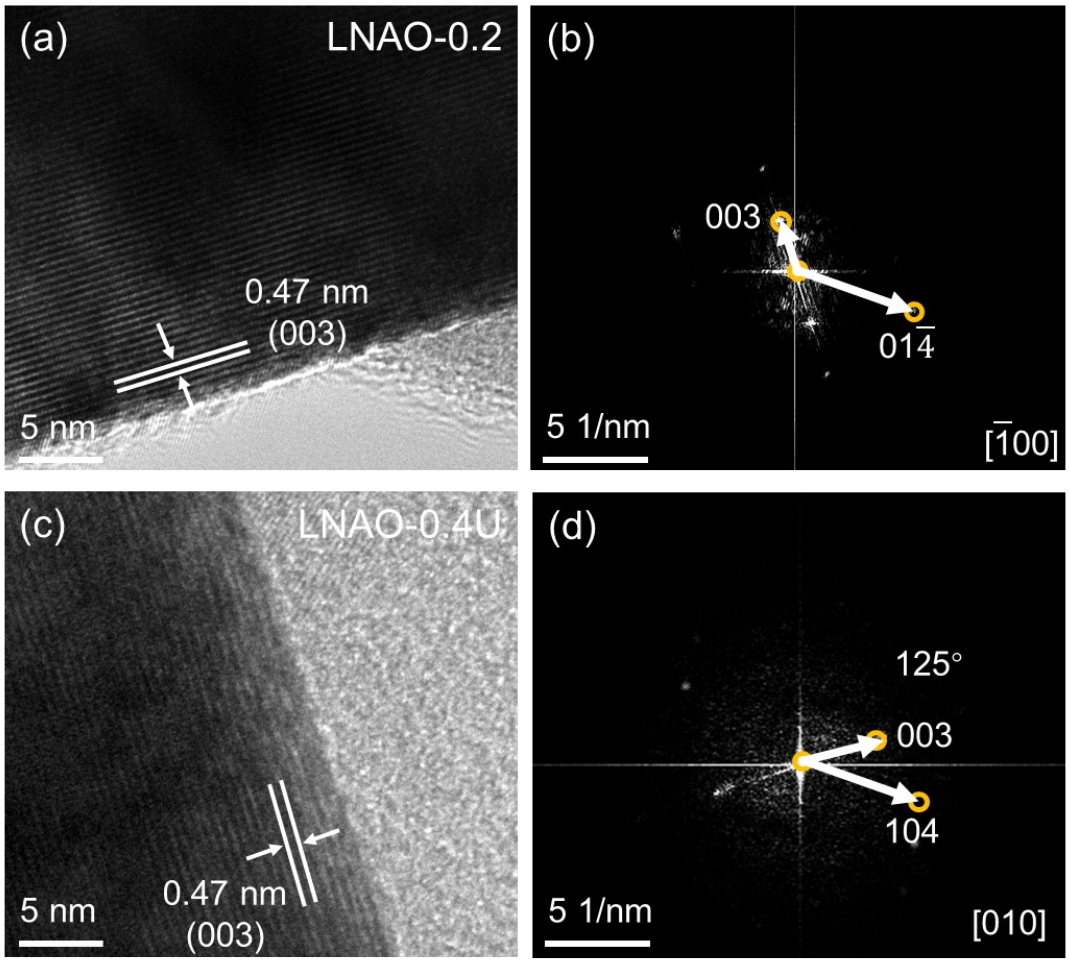

Figure S7. HRTEM images and FFT patterns of (a, b) LNAO-0.2, (c, d) LNAO-0.4U.

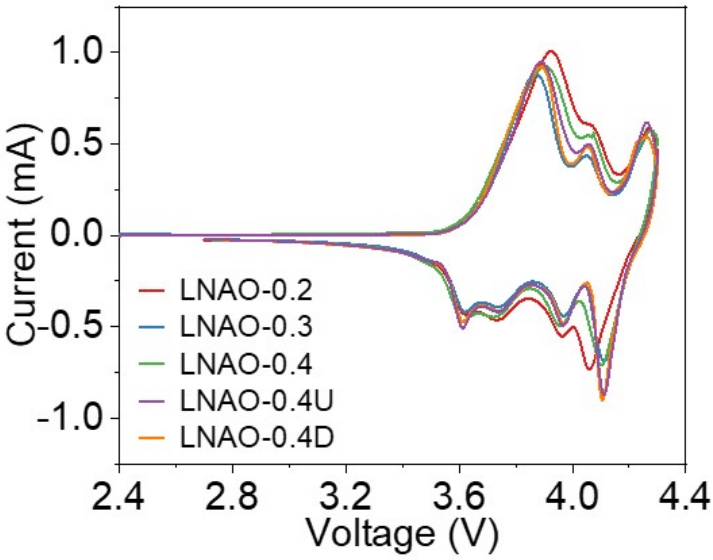

Figure S8. CV curves of LNAO cathodes in the voltage range of 2.7 – 4.3 V.

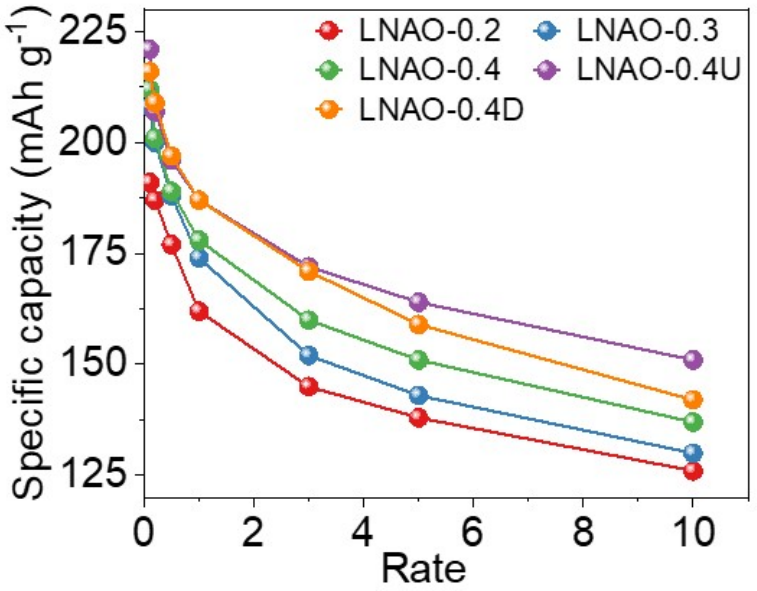

Figure S9. Rate performance of LNAO cathodes.

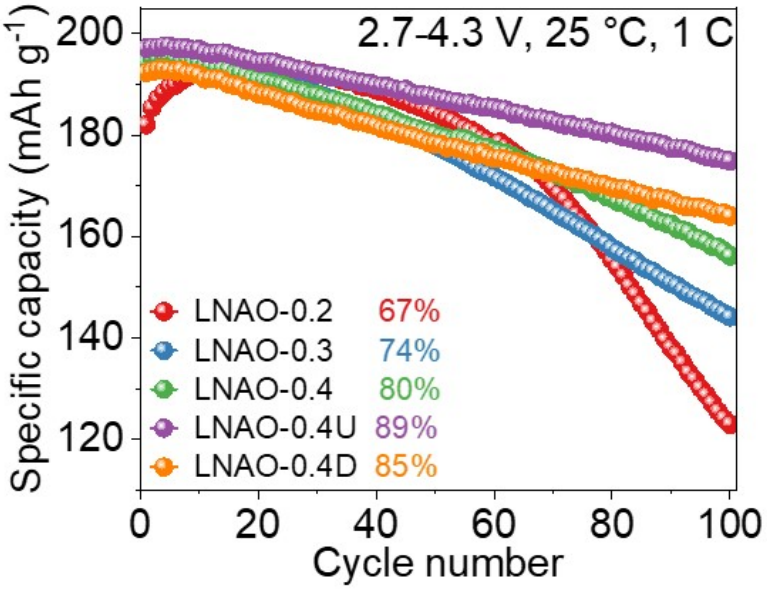

Figure S10. The cyclability of LNAO cathodes at 1 C in the voltage range of 2.7 – 4.3 V.

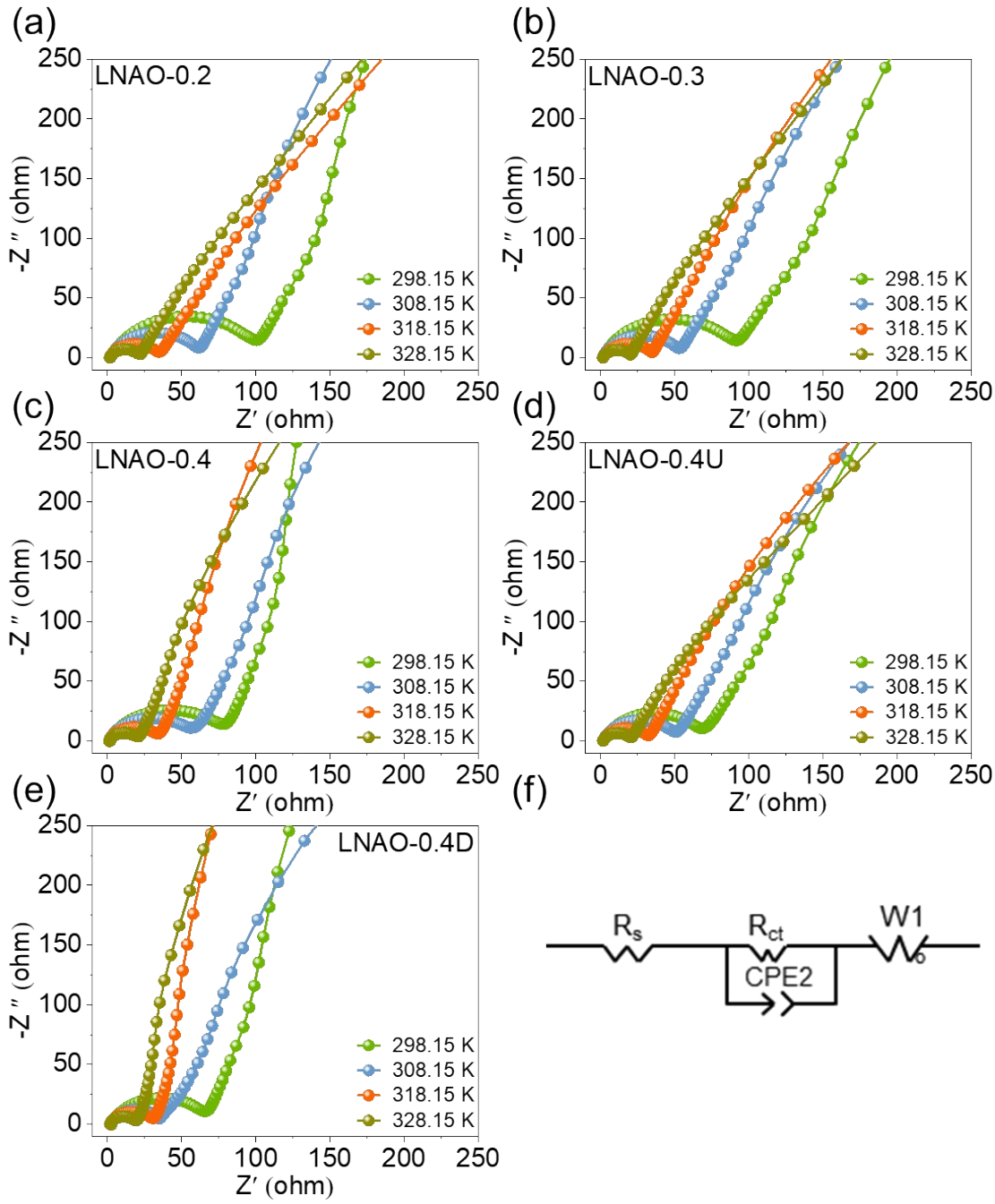

Figure S11. Nyquist plots of (a) LNAO-0.2, (b) LNAO-0.3, (c) LNAO-0.4, (d) LNAO-0.4U and (e) LNAO-0.4D at different temperatures; (f) equivalent circuit models used in impedance fitting.

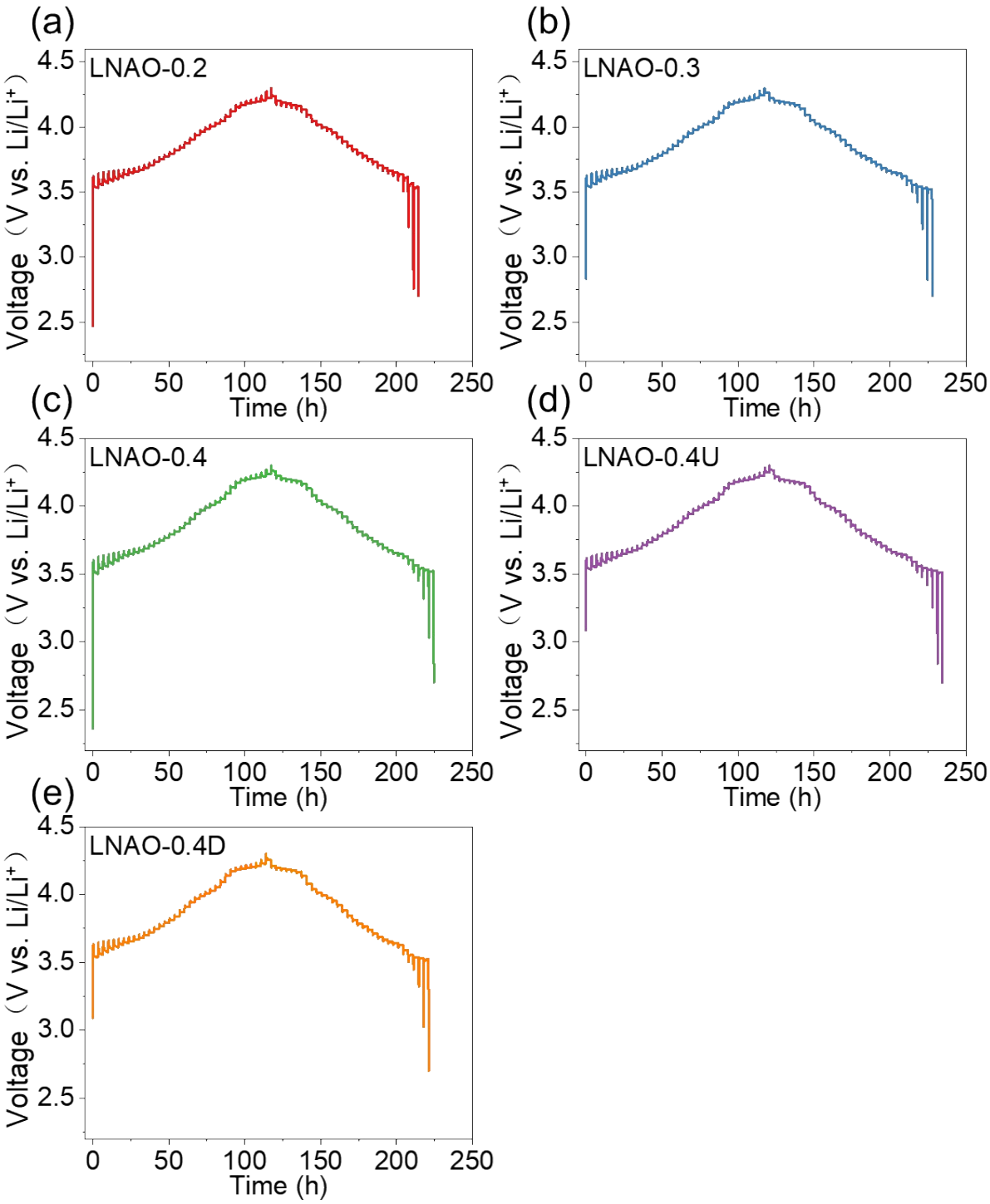

Figure S12. GITT profiles of (a) LNAO-0.2, (b) LNAO-0.3, (c) LNAO-0.4, (d) LNAO-0.4U, (e) LNAO-0.4D.

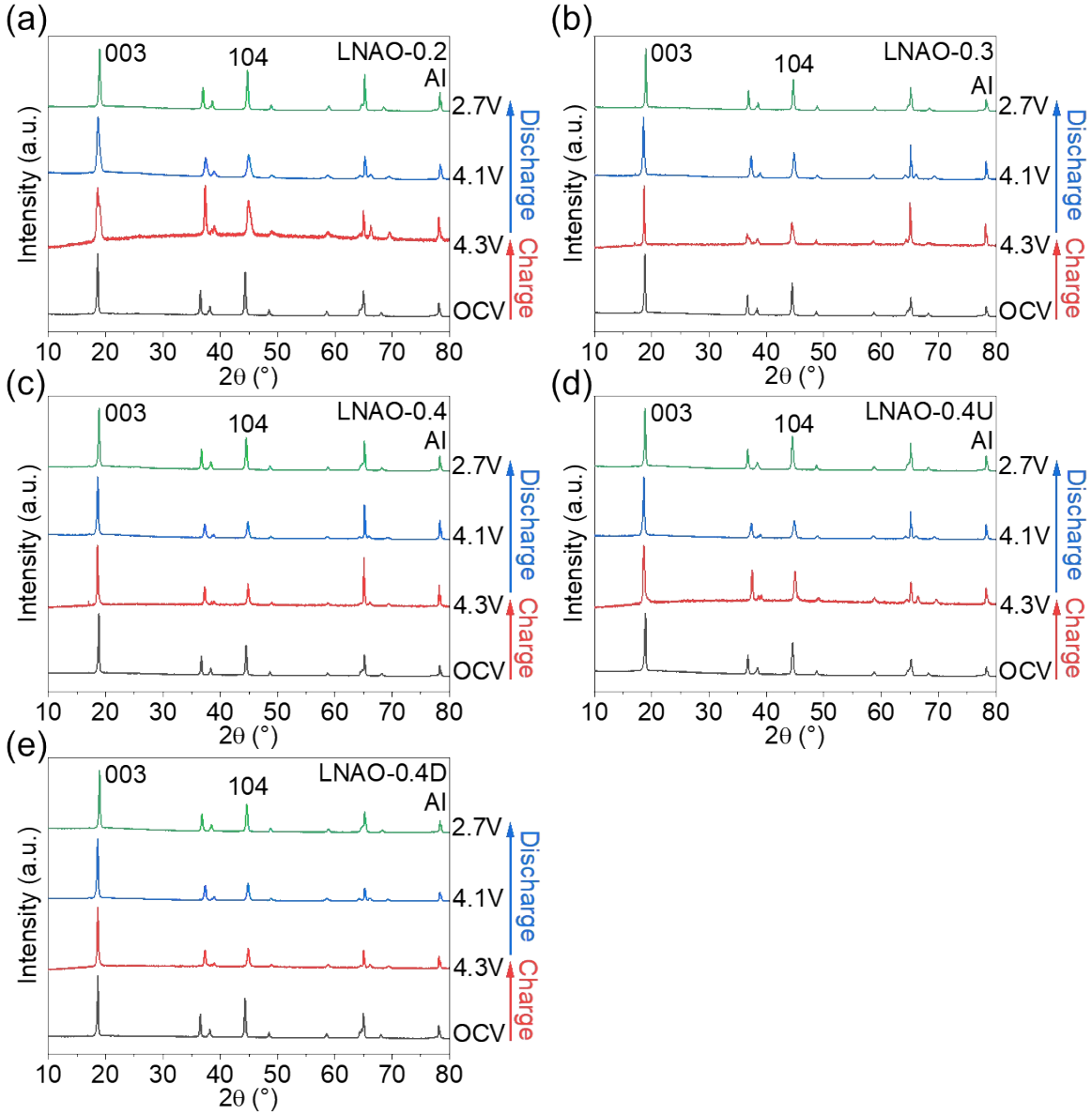

Figure S13. XRD pattern of (a) LNAO-0.2, (b) LNAO-0.3, (c) LNAO-0.4, (d) LNAO-0.4U and (e) LNAO-0.4D at various charge/discharge states.

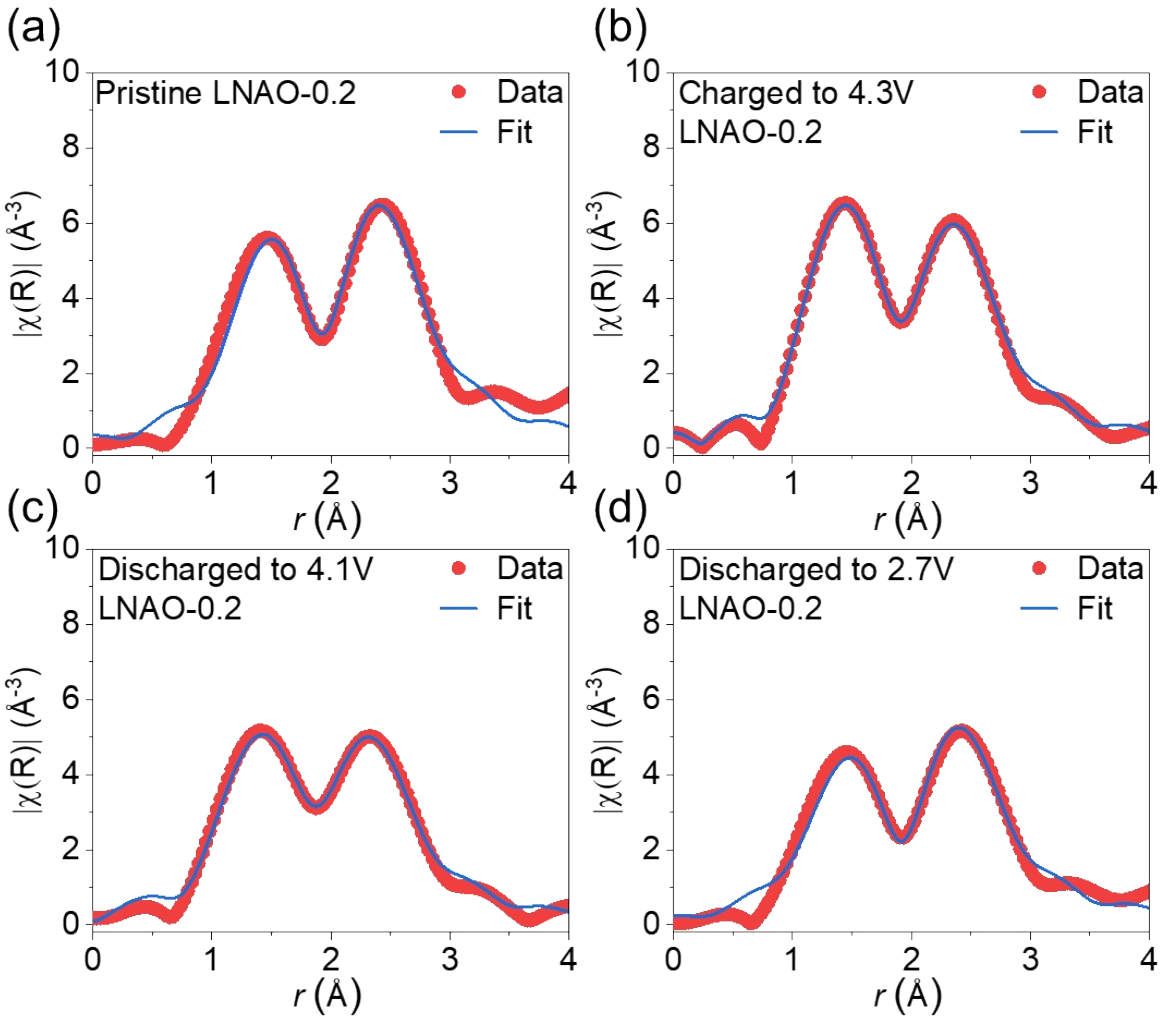

Figure S14. k^2-weighted Fourier transform magnitude and the Fitting of Ni K-edge EXAFS spectra for LNAO-0.2 at various charge/discharge states. (a) Pristine LNAO-0.2; (b) Charged to 4.3 V; (c) Discharged to 4.1 V; (d) Discharged to 2.7 V.

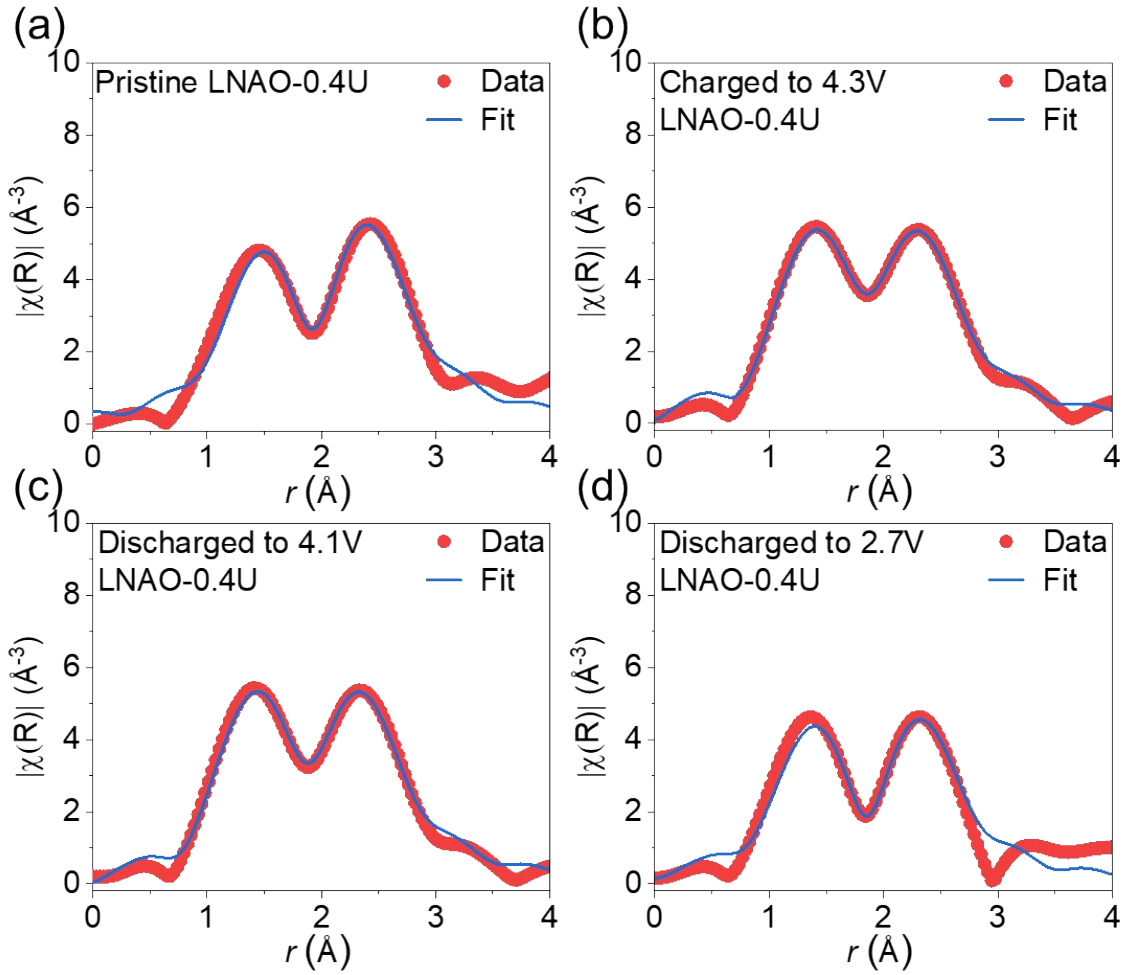

Figure S15. k^2-weighted Fourier transform magnitude and the Fitting of Ni K-edge EXAFS spectra for LNAO-0.4U at various charge/discharge states. (a) Pristine LNAO-0.2; (b) Charged to 4.3 V; (c) Discharged to 4.1 V; (d) Discharged to 2.7 V.

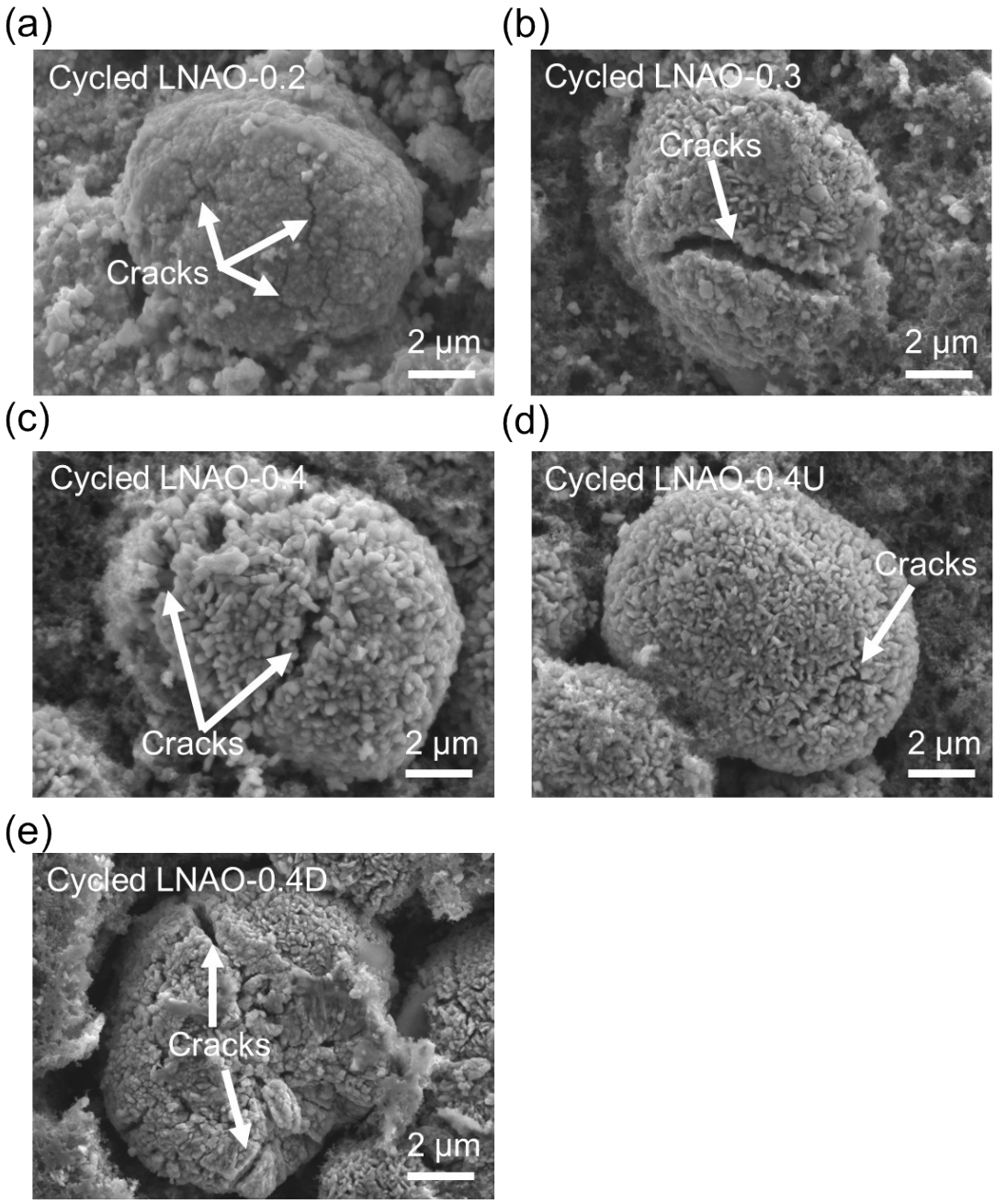

Figure S16. SEM images of (a) LNAO-0.2, (b) LNAO-0.3, (c) LNAO-0.4, (d) LNAO-0.4U and (e) LNAO -0.4D after 100 cycles at 1C.

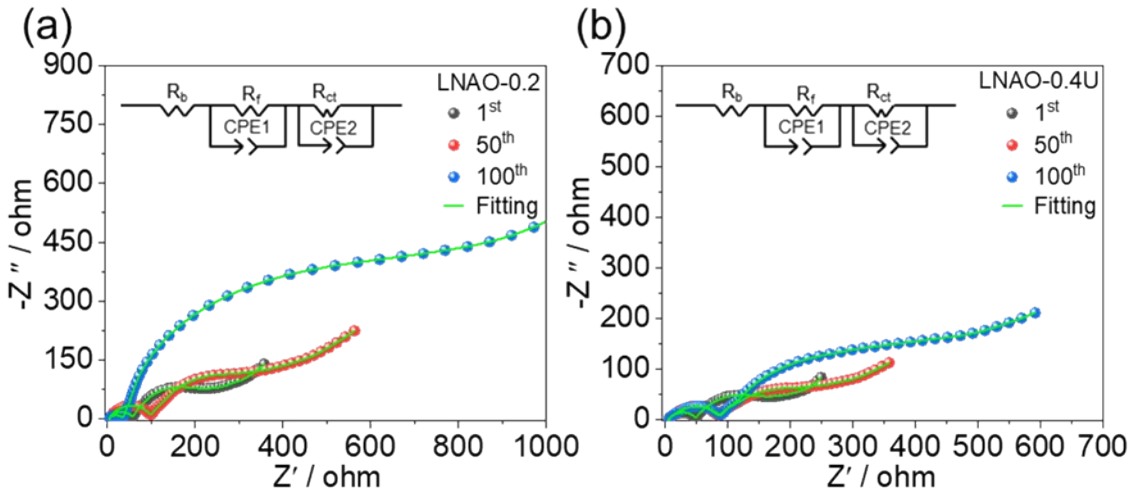

Figure S17. Nyquist plots of LNAO-0.2 and LNAO-0.4U in the discharged state after 1, 50 and 100 cycles, and the inset in Figure is equivalent circuit spectrogram.

The electrochemical impedance spectra of LNAO-0.2 and LNAO-0.4U at varying cycle counts are presented in Figure S17. The Nyquist plots were analyzed using equivalent circuit modeling, with the resulting impedance data summarized in Table S16. Throughout the cycling process, both the ohmic resistance (R_b) and the surface film resistance (R_f) remained relatively stable. However, the charge-transfer resistance (R_{ct}) exhibited notable changes. Specifically, for the LNAO-0.2 electrodes, the R_{ct} increased from approximately 27 Ω during the initial cycle to about 421 Ω after 100 cycles. In contrast, the LNAO-0.4U electrode showed a more modest increase, rising from approximately 20 Ω in the initial cycle to around 128 Ω after 100 cycles. This smaller increase in R_{ct} for the LNAO-0.4U electrode may be attributed to its plate-like primary particles, which help mitigate microstrain and reduce the occurrence of microcracks and surface side reactions.

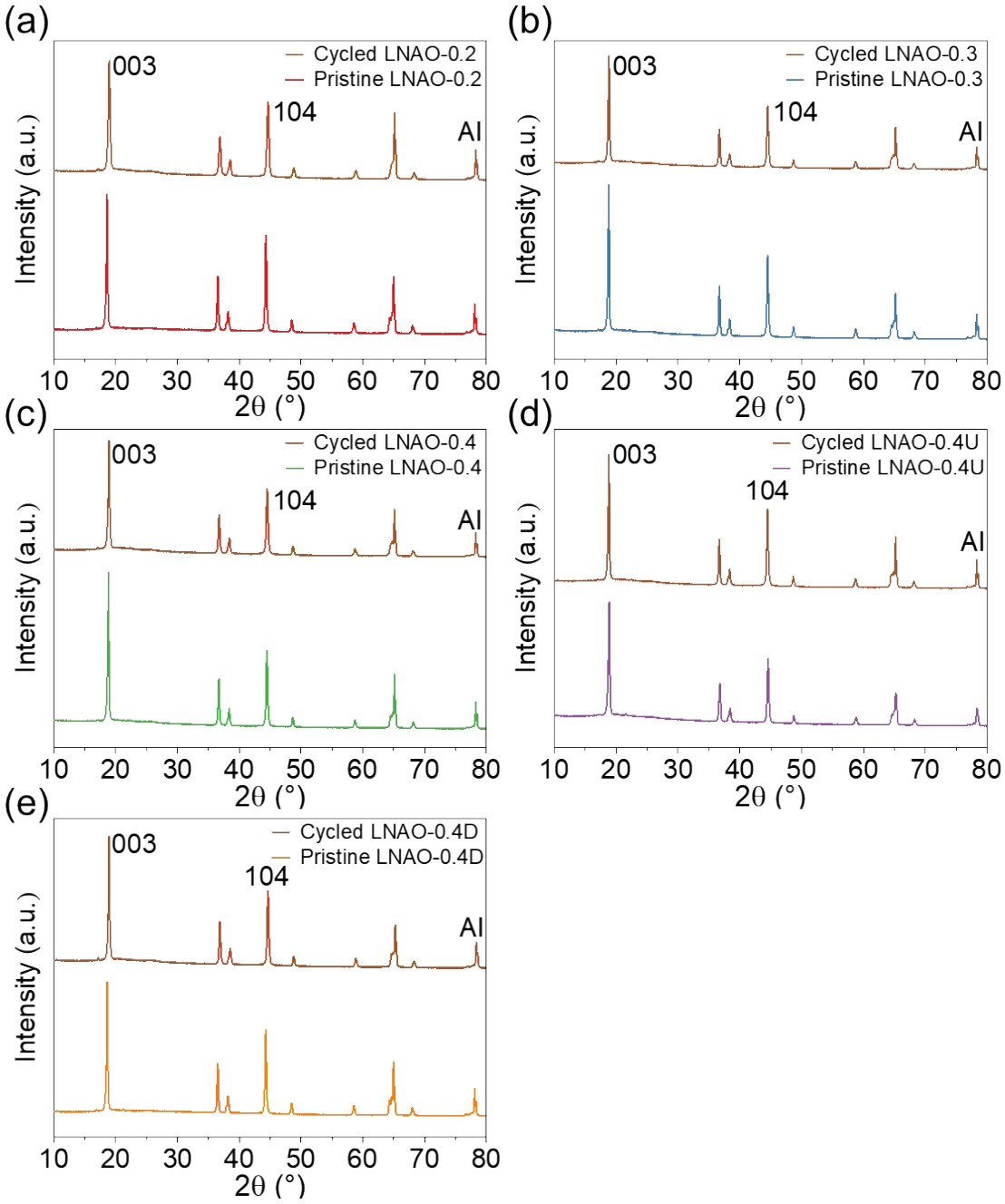

Figure S18. Comparison of XRD patterns of electrodes before cycling and after 100 cycles at 1C: (a) LNAO-0.2, (b) LNAO-0.3, (c) LNAO-0.4, (d) LNAO-0.4U, (e) LNAO -0.4D.

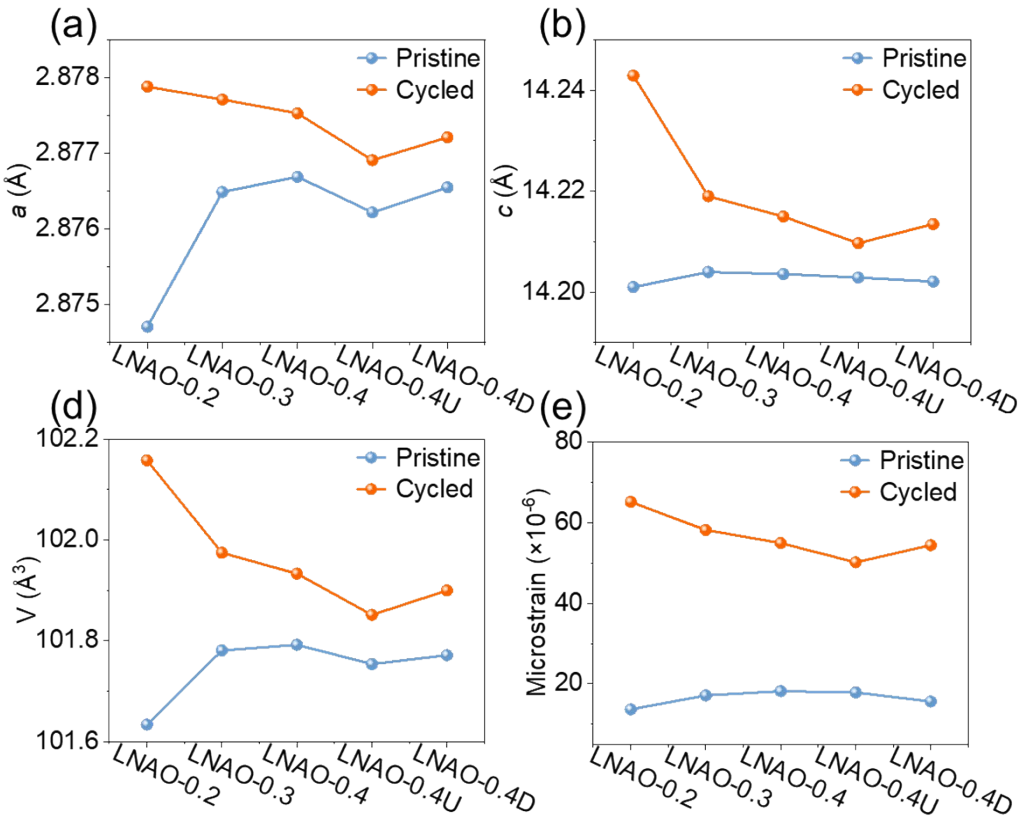

Figure S19. Lattice parameters (a) *a*, (b) *c* and (c) unit cell volume *V* of the electrodes before and after cycling; (d) the microstrain of LNAO cathodes before and after cycling

Table S1. The nucleation rate (B^0) of all hydroxide precursors during synthesis

Precursors	5 h	10 h	15 h	20 h	25 h	30 h
NH-0.2/Number m^{-3} s^{-1}	7.46×10^{13}	4.89×10^{14}	5.78×10^{14}	6.89×10^{14}	7.60×10^{14}	8.45×10^{14}
NH-0.3/Number m^{-3} s^{-1}	2.39×10^{13}	3.95×10^{13}	4.38×10^{13}	2.24×10^{14}	2.20×10^{14}	1.83×10^{14}
NH-0.4/Number m^{-3} s^{-1}	1.90×10^{9}	1.28×10^{13}	2.52×10^{13}	2.47×10^{14}	1.98×10^{14}	1.51×10^{14}
NH-0.4U/Number m^{-3} s^{-1}	2.44×10^{10}	2.66×10^{8}	2.15×10^{9}	3.09×10^{9}	5.43×10^{9}	1.05×10^{10}
NH-0.4D/Number m^{-3} s^{-1}	1.78×10^{9}	1.00×10^{10}	4.52×10^{11}	4.21×10^{12}	3.88×10^{13}	1.37×10^{14}

Table S2. The inductively coupled plasma mass spectrometer (ICP-MS) results of LNAO-0.2, LNAO-0.3, LNAO-0.4, LNAO-0.4U, and LNAO-0.4D.

Samples	Li	Ni	Al
LNAO-0.2	1.001	0.953	0.051
LNAO-0.3	0.999	0.950	0.050
LNAO-0.4	1.001	0.952	0.049
LNAO-0.4U	1.001	0.951	0.050
LNAO-0.4D	1.002	0.950	0.051

Table S3. Rietveld refinement results of the samples.

Samples	*a* (Å)	*c* (Å)	*V* (Å^3)	*c*/*a*
NC	2.8747(2)	14.2011(3)	101.6333(6)	4.9401
NCA1	2.8765(2)	14.2041(3)	101.7808(6)	4.9380
NCA2	2.8767(2)	14.2036(3)	101.7921(6)	4.9375
NCA3	2.8762(2)	14.2029(3)	101.7538(6)	4.9380
NA	2.8766(2)	14.2021(3)	101.7714(6)	4.9372

Table S4. Crystallographic parameters of LNAO-0.2.

Cell parameters

Space group: $R\bar{3}m$, $a = b = 2.8747(2)$ Å, $c = 14.2011(3)$ Å, $V = 101.6333(6)$ Å^3,

alpha = *beta* = 90°, *gamma* = 120°

Atomic positions

Name	site	*x*	*y*	*z*	Fract
O1	6*c*	0.000	0.000	0.250	1.000
Li1	3*a*	0.000	0.000	0.000	0.974
Ni2	3*a*	0.000	0.000	0.000	0.026
Ni1	3*b*	0.000	0.000	0.500	0.924
Al	3*b*	0.000	0.000	0.500	0.050
Li2	3*b*	0.000	0.000	0.500	0.026

Refinement parameters

R_{wp}= 2.73 %, R_p= 3.50 %, χ^2: 1.2

Note: Fract is the fractional occupancy of the atom on this site.

Table S5. Crystallographic parameters of LNAO-0.3.

Cell parameters

Space group: $R\bar{3}m$, $a = b = 2.8765(2)$ Å, $c = 14.2041(3)$ Å, $V = 101.7808(6)$ Å^3,

alpha = *beta* = 90°, *gamma* = 120°

Atomic positions

Name	site	*x*	*y*	*z*	Fract
O1	6*c*	0.000	0.000	0.250	1.000
Li1	3*a*	0.000	0.000	0.000	0.976
Ni2	3*a*	0.000	0.000	0.000	0.024
Ni1	3*b*	0.000	0.000	0.500	0.926
Al	3*b*	0.000	0.000	0.500	0.050
Li2	3*b*	0.000	0.000	0.500	0.024

Refinement parameters

R_{wp}= 2.88 %, R_p= 3.61 %, χ^2: 1.26

Table S6. Crystallographic parameters of LNAO-0.4.

Cell parameters

Space group: $R\bar{3}m$, $a = b = 2.8767(2)$ Å, $c = 14.2036(3)$ Å, $V = 101.7921(6)$ Å^3,

alpha = *beta* = 90°, *gamma* = 120°

Atomic positions

Name	site	*x*	*y*	*z*	Fract
O1	6*c*	0.000	0.000	0.250	1.000
Li1	3*a*	0.000	0.000	0.000	0.975
Ni2	3*a*	0.000	0.000	0.000	0.025
Ni1	3*b*	0.000	0.000	0.500	0.925
Al	3*b*	0.000	0.000	0.500	0.050
Li2	3*b*	0.000	0.000	0.500	0.025

Refinement parameters

R_{wp}= 2.71 %, R_p= 3.50 %, χ^2: 1.20

Table S7. Crystallographic parameters of LNAO-0.4U.

Cell parameters

Space group: $R\bar{3}m$, $a = b = 2.8762(2)$ Å, $c = 14.2029(3)$ Å, $V = 101.7538(6)$ Å^3,

alpha = *beta* = 90°, *gamma* = 120°

Atomic positions

Name	site	*x*	*y*	*z*	Fract
O1	6*c*	0.000	0.000	0.250	1.000
Li1	3*a*	0.000	0.000	0.000	0.974
Ni2	3*a*	0.000	0.000	0.000	0.026
Ni1	3*b*	0.000	0.000	0.500	0.924
Al	3*b*	0.000	0.000	0.500	0.050
Li2	3*b*	0.000	0.000	0.500	0.026

Refinement parameters

R_{wp}= 2.91 %, R_p= 3.66 %, χ^2: 1.27

Table S8. Crystallographic parameters of LNAO-0.4D.

Cell parameters

Space group: $R\bar{3}m$, $a = b = 2.8766(2)$ Å, $c = 14.2021(3)$ Å, $V = 101.7714(6)$ Å^3,

alpha = *beta* = 90°, *gamma* = 120°

Atomic positions

Name	site	*x*	*y*	*z*	Fract
O1	6*c*	0.000	0.000	0.250	1.000
Li1	3*a*	0.000	0.000	0.000	0.977
Ni2	3*a*	0.000	0.000	0.000	0.023
Ni1	3*b*	0.000	0.000	0.500	0.927
Al	3*b*	0.000	0.000	0.500	0.050
Li2	3*b*	0.000	0.000	0.500	0.023

Refinement parameters

R_{wp}= 2.70 %, R_p= 3.50 %, χ^2: 1.49

Table S9. Rate performances of the electrodes.

Electrodes	0.1 C	0.2 C	0.5 C	1 C	3 C	5 C	10 C
LNAO-0.2/mAh g^{-1}	191	187	177	162	145	138	126
LNAO-0.3/mAh g^{-1}	208	200	188	174	152	143	130
LNAO-0.4/mAh g^{-1}	212	201	189	178	160	151	137
LNAO-0.4U/mAh g^{-1}	221	207	196	187	172	164	151
LNAO-0.4D/mAh g^{-1}	216	209	197	187	171	159	142

Table S10. Charge/discharge capacity and coulomb efficiency (CE) at 0.1C

Electrodes	Charge specific capacity/mAh g^{-1}	Discharge specific capacity/mAh g^{-1}	1st cycle CE
LNAO-0.2	238	191	80%
LNAO-0.3	238	208	87%
LNAO-0.4	241	212	88%
LNAO-0.4U	241	221	91%
LNAO-0.4D	242	216	89%

Table S11. Energy density of the electrodes.

Item	LNAO-02	LNAO-0.3	LNAO-0.4	LNAO-0.4U	LNAO-0.4D
Energy density ($Wh\ kg^{-1}$)	742	803	820	850	834

Table S12. Calculated apparent activation energies (E_a) for lithium ion insertion into different cathode materials.

Item	LNAO-02	LNAO-0.3	LNAO-0.4	LNAO-0.4U	LNAO-0.4D
E_a (eV)	0.43 ± 0.02	0.40 ± 0.02	0.38 ± 0.02	0.33 ± 0.02	0.34 ± 0.02

Table S13. Capacity retentions of the electrodes at 1C.

Item	LNAO-02	LNAO-0.3	LNAO-0.4	LNAO-0.4U	LNAO-0.4D
Capacity retention after 100 cycles	67%	74%	80%	89%	85%

Table S14. Curve fitting results for the Ni K-edge EXAFS spectra of LNAO-0.2 at different charge/discharge states.

State	Bond	CN	σ^2 (Å^2)	S_0^2	R(Å)	R-factor
Pristine	Ni-O	6	0.0068(1)	0.68	1.946(5)	0.0056
	Ni-TM	6	0.0040(1)	0.68	2.878(5)	0.0056
Charge to 4.3 V	Ni-O	6	0.0021(1)	0.68	1.876(5)	0.0053
	Ni-TM	6	0.0027(1)	0.68	2.829(5)	0.0053
Discharge to 4.1 V	Ni-O	6	0.0026(1)	0.68	1.883(5)	0.0094
	Ni-TM	6	0.0033(1)	0.68	2.828(5)	0.0094
Discharged to 2.7 V	Ni-O	6	0.0091(1)	0.68	1.936(5)	0.0047
	Ni-TM	6	0.0057(1)	0.68	2.872(5)	0.0047

Table S15. Curve fitting results for the Ni K-edge EXAFS spectra of LNAO-0.4U at different charge/discharge states.

State	Bond	CN	σ^2 (Å^2)	S_0^2	R(Å)	R-factor
Pristine	Ni-O	6	0.0067(1)	0.68	1.947(5)	0.0076
	Ni-TM	6	0.0043(1)	0.68	2.878(5)	0.0076
Charge to 4.3 V	Ni-O	6	0.0015(1)	0.68	1.879(5)	0.0093
	Ni-TM	6	0.0025(1)	0.68	2.834(5)	0.0093
Discharge to 4.1 V	Ni-O	6	0.0022(1)	0.68	1.886(5)	0.0016
	Ni-TM	6	0.0027(1)	0.68	2.831(5)	0.0016
Discharged	Ni-O	6	0.0085(1)	0.68	1.942(5)	0.0022
	Ni-TM	6	0.0077(1)	0.68	2.875(5)	0.0022

Table S16 Fitting results of equivalent circuit from Nyquist curves in **Figure** S17.

Samples	Cycles	R_b (Ω)	R_f (Ω)	R_{ct} (Ω)
LNAO-0.2	1st	4 ± 1	22 ± 5	27 ± 5
	50th	4 ± 1	31 ± 5	112 ± 10
	100th	4 ± 1	39 ± 5	421± 10
LNAO-0.4U	1st	3 ± 1	25 ± 5	20 ± 5
	50th	3 ± 1	35 ± 5	26 ± 5
	100th	3 ± 1	38 ± 5	128 ± 10